ACS APPLIED MATERIALS & INTERFACES

www.acsami.org

Research Article

Genetically Engineered Protein-Based Bioadhesives with Programmable Material Properties

Juya Jeon, Kok Zhi Lee, Xiaolu Zhang, John Jaeger, Eugene Kim, Jingyao Li, Larisa Belaygorod, Batool Arif, Guy M. Genin, Marcus B. Foston, Mohamed A. Zayed, and Fuzhong Zhang*

Cite This: *ACS Appl. Mater. Interfaces* 2023, 15, 56786−56795

Read Online

ACCESS | Metrics & More | Article Recommendations | Supporting Information

ABSTRACT: Silk-amyloid-mussel foot protein (SAM) hydrogels made from recombinant fusion proteins containing β-amyloid peptide, spider silk domain, and mussel foot protein (Mfp) are attractive bioadhesives as they display a unique combination of tunability, biocompatibility, bioabsorbability, strong cohesion, and underwater adhesion to a wide range of biological surfaces. To design tunable SAM hydrogels for tailored surgical repair applications, an understanding of the relationships between protein sequence and hydrogel properties is imperative. Here, we fabricated SAM hydrogels using fusion proteins of varying lengths of silk-amyloid repeats and Mfps to characterize their structure and properties. We found that increasing silk-amyloid repeats enhanced the hydrogel's β-sheet content (r = 0.74), leading to higher cohesive strength and toughness. Additionally, increasing the Mfp length beyond the half-length of the full Mfp sequence (1/2 Mfp) decreased the β-sheet content (r = −0.47), but increased hydrogel surface adhesion. Among different variants, the hydrogel made of 16xKLV-2Mfp displayed a high ultimate strength of 3.0 ± 0.3 MPa, an ultimate strain of 664 ± 119%, and an attractive underwater adhesivity of 416 ± 20 kPa to porcine skin. Collectively, the sequence-structure−property relationships learned from this study will be useful to guide the design of future protein adhesives with tunable characteristics for tailored surgical applications.

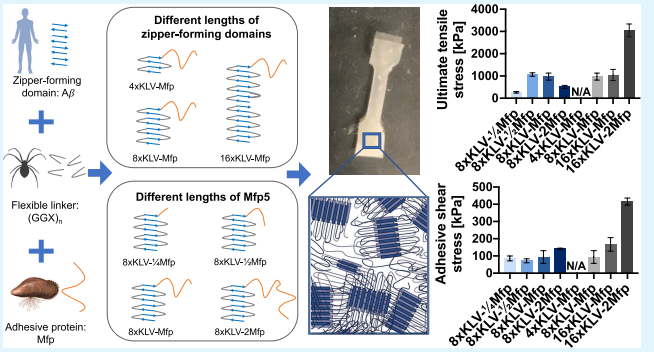

KEYWORDS: *underwater adhesive, bioadhesive, protein materials, programmable material properties, amyloid beta-peptides, mussel foot protein, synthetic biology*

INTRODUCION

Biocompatible and bioabsorbable adhesives are urgently needed for multiple internal biomedical applications such as tissue repair, surgical glues, drug release vehicles, etc.[1−3] Such adhesives need to display strong adhesion to wet biological tissues and mechanical properties (i.e., modulus, tensile/compressive strength, elasticity, etc.) that match the target tissue. Several types of commercial bioglues have been recently developed, including cyanoacrylates, polyester-based adhesives, and poly(acrylic acid)-based glues.[4−8] Most bioglues are synthetic polymers with limited biodegradability, high toxicity, and lack of tunability.[9−11] Furthermore, many existing bioglues do not have desirable adhesion to wet biological tissues, thus limiting their practical use.[2,12,13] A class of bioglues that has not been extensively explored are those that are completely made of proteins.[14,15] Protein-based adhesives are generally biocompatible and bioabsorbable as many protein-based biomaterials have been used for biomedical applications.[1,3,16−18] Additionally, recombinant proteins synthesized from DNA templates allow their protein sequences to be precisely controlled, enabling fine-tuning of mechanical and adhesive properties to match specific requirements for biomedical applications.[8,17,19,20] These features are hardly achieved by other materials.

One attractive protein-based adhesive is the silk-amyloid-mussel foot protein (SAM) hydrogel that displays a unique combination of high adhesion and mechanical properties for surgical repairs.[21] The SAM hydrogel is made of an artificially designed fusion protein, produced from engineered microbes. In the SAM hydrogel, the silk-amyloid repeats self-assemble into needle-like β-sheet nanocrystals[21−23] and the disordered mussel foot protein (Mfp) forms intermolecular interactions as well as protein−surface interactions, which contributes to the hydrogel's cohesive properties and surface adhesion, respectively.[21,24,25] The modular SAM sequence design offers a high level of material tunability. The number of silk-amyloid repeats can potentially control the size and amount of β-sheet

Received: August 31, 2023
Revised: October 23, 2023
Accepted: November 17, 2023
Published: December 1, 2023

https://doi.org/10.1021/acsami.3c12919
ACS Appl. Mater. Interfaces 2023, 15, 56786−56795

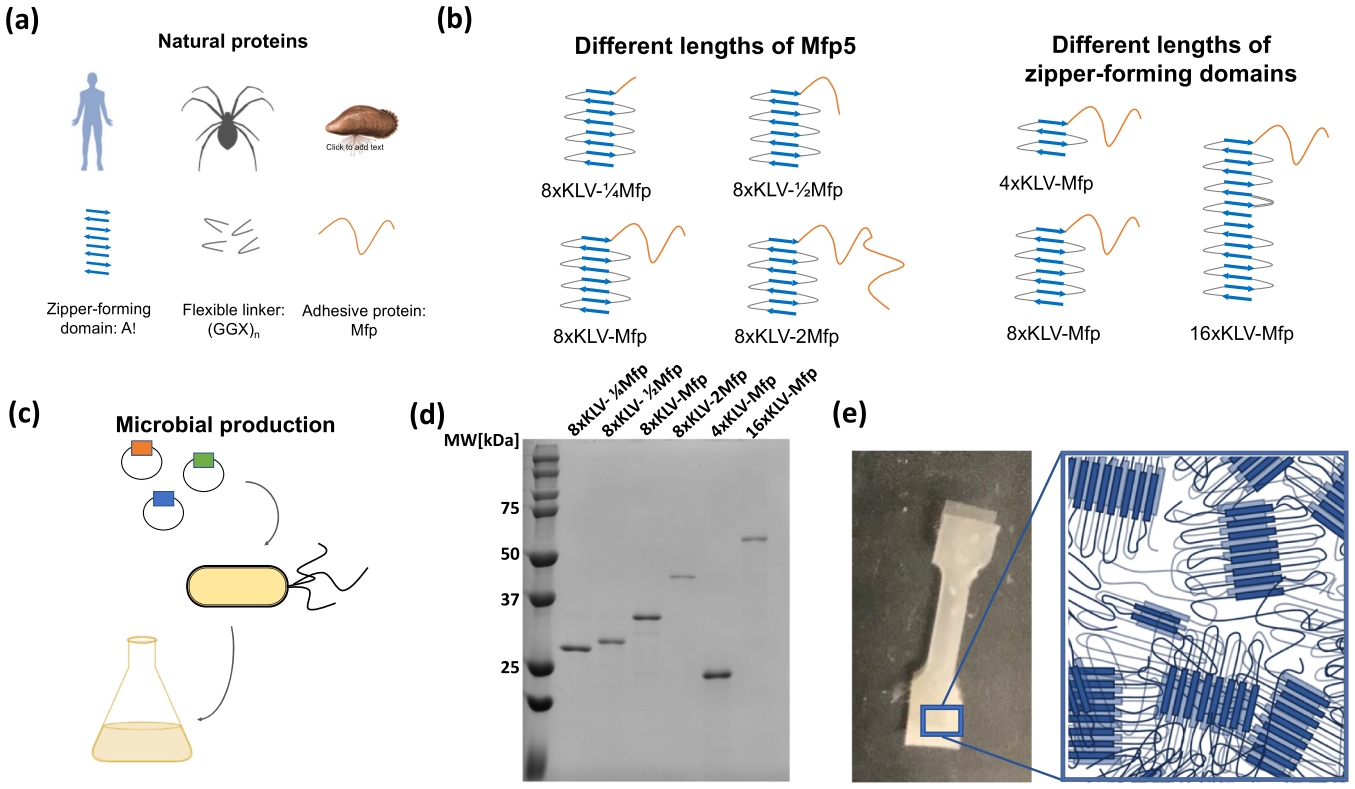

Figure 1. SAM proteins with different sequences. (a) Schematic showing the design of SAM proteins. (b) Design of different protein variants. The first group of variants includes SAM proteins with different lengths of Mfp. The second group of variants includes SAMs with different numbers of silk-amyloid repeats. (c) Schematic showing the expression of SAM protein variants. Plasmids of variants were transformed to NEB10B *E. coli* and cultured through microbial production. (d) Representative SDS-PAGE gel of purified SAM proteins. (e) Representative image of SAM hydrogel in a dogbone shape and the proposed protein structure. Striped rectangles represent β-nanocrystals.

nanocrystals, while the length of Mfp can potentially vary intermolecular interaction and surface adhesion. However, changing the nanocrystal size unavoidably influences Mfp−Mfp interaction, and varying Mfp length may affect the folding of β-sheet nanocrystals. It is thus essential to understand the relationship between protein sequence with hydrogel structure and properties, which will help build design rules for engineering desirable bioglues to match specific applications and even personalized adhesives.

To achieve this goal, here, we designed multiple SAM proteins with varying lengths of either silk-amyloid repeats or Mfp. These proteins were produced and processed into hydrogels followed by material characterization. We found that for proteins with fixed Mfp lengths, increasing silk-amyloid repeats resulted in hydrogels with higher β-sheet content, higher cohesive strength and toughness, and higher adhesion. For proteins with fixed 8 repeats of the silk-amyloid domain (8xKLV), a longer Mfp length beyond 1/2 Mfp leads to decreased β-sheet content but higher adhesion. We observed a high correlation between the number of silk-amyloid repeats with the β-sheet content and hydrogel cohesive strength. The sequence-structure−property relationships elucidated by this study can be used to guide the design of future protein adhesives with tunable properties to tailor specific applications. Additionally, one hydrogel, 16xKLV-2Mfp, displayed a high ultimate strength of 3.0 ± 0.3 MPa, an ultimate strain of 664 ± 119%, and an attractive underwater adhesion of 416 ± 20 kPa to porcine skin.

RESULTS AND DISCUSSION

Design and Synthesis of SAM Variant hydrogels. Previous SAM proteins were designed by connecting a β-sheet-forming amyloid peptide (KLVFFAE) with a flexible silk sequence (GGAGQGGYGGLGSQGTSGRGGLGGQGAG) from the amorphous region of the *Nephila clavipes* dragline spider silk protein MaSp1. The silk-amyloid sequence was alternately repeated eight times, followed by fusion with Mfp5 at the C-terminus, resulting in the 8xKLV-Mfp protein. To understand the effect of different domains, we designed SAM variants to investigate the roles of both silk-amyloid and Mfp separately. We first varied the Mfp length by either truncating or duplicating the Mfp sequence, resulting in 8xKLV-1/4Mfp, 8xKLV-1/2Mfp, and 8xKLV-2Mfp that contain a quarter, half, and two repeats of Mfp sequence, respectively. We further varied the length of silk-amyloid, resulting in 4xKLV-Mfp and 16xKLV-Mfp that contain 4 and 16 silk-amyloid repeats, respectively. Finally, 16xKLV-2Mfp was synthesized by fusing two repeats of Mfp to 16 silk-amyloid repeats (Figures 1b and S1).

We used our rapid cloning strategy and synthetic biology platform to produce these proteins.[21,26−28] All proteins were produced and purified to high purities (>90%) (Figure 1d). Purified proteins were used to fabricate hydrogels following published methods for 8xKLV-Mfp (Figure 1c).[21] All SAM variants formed strong hydrogels except for 4xKLV-Mfp, suggesting that 4xKLV is too short to form crystalline nanoscaffolds that are crucial for ordered interactions between Mfp sequences.[21]

Structural Characterization of Different SAM Hydrogels. Environmental scanning electron microscopy (ESEM)

https://doi.org/10.1021/acsami.3c12919
ACS Appl. Mater. Interfaces 2023, 15, 56786−56795

was used to study the surface morphology of SAM hydrogels. All hydrogels have similar surface morphologies and porosities (Figure 2), suggesting that these sequence changes do not affect

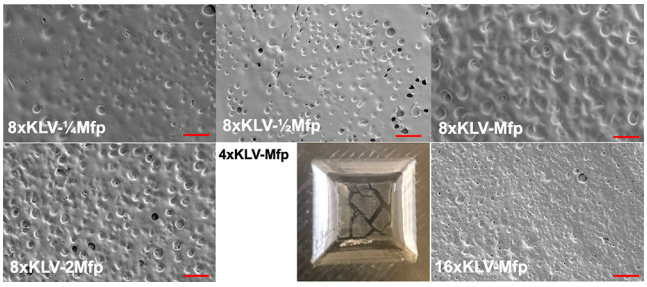

Figure 2. Representative SEM images of SAM hydrogels. Images showing the surface of the fabricated hydrogel of each SAM protein variant using SEM. The red bars on the images represent 100 μm. While other hydrogels were successfully fabricated, 4xKLV-Mfp protein failed to form hydrogel under our experimental conditions—the image of 4xKLV-Mfp shows broken hydrogel pieces in the PDMS mold due to fabrication failure.

surface morphology. To understand sequence-structure relationships, Fourier-transform infrared spectroscopy (FTIR) was used to examine hydrogel secondary structures. All hydrogels displayed a strong amide I band at 1600−1700 cm^{-1} (Figure 3a).[22,29] Deconvolution of this peak revealed that these hydrogels have different amounts of β-sheets (Figure 3b). For hydrogels containing the 8xKLV sequence, β-sheet content decreases when the Mfp length increases except 8KLV-1/4 Mfp. For hydrogels containing full-length Mfp, the β-sheet content increases as KLV repeats increase (Figure 3b,c). These observations are consistent with our hypothesis that a higher number of silk-amyloid repeats promotes β-sheet formation while the disordered Mfp negatively affects β-sheet folding. Next, we stained the hydrogels with Congo Red, which emits a red fluorescence upon binding to amyloid fibrils.[30,31] Similar to β-sheet contents, a higher number of KLV repeats promotes amyloid formation, while a longer Mfp sequence decreases amyloid formation (Figure 3d,e). Thus, both FTIR and Congo Red staining showed that the cross-β structures are formed by silk-amyloid repeats and can be enhanced by increasing the repeat number. At the same time, too long Mfp sequence can disrupt the formation of β-sheets, potentially lowering the degree of crystallinity.

Mechanical Characterization of Different Hydrogels. Standard tensile tests were performed to examine the mechanical properties of the SAM hydrogels (Figure 4a). The 8xKLV-1/4 Mfp hydrogel is weak and relatively brittle, displaying an ultimate strength of 265 ± 34 kPa and an ultimate strain of 26 ± 9% (Figures 4b−d and S4a). This suggests that 1/4 Mfp is too short to form extensive intermolecular interactions. The 8xKLV-1/2 Mfp hydrogel, on the other hand, has dramatically higher ultimate strength and strain, reaching 1.07 ± 0.08 MPa and 276 ± 47%, respectively. This indicates that 1/2 Mfp has sufficient length to provide strong intermolecular interactions. However, when Mfp length further increases from 1/2 Mfp to 2 Mfp, hydrogel strength and strain decrease (Figure 4b,c). This trend matches with the change of β-sheet content, suggesting that with sufficient intermolecular interaction (beyond 1/2 Mfp), a longer Mfp sequence on 8xKLV leads to a lower β-sheet content and reduced hydrogel strength (Figure 4g,h).

Meanwhile, for hydrogels containing full-length Mfp, as the number of silk-amyloid repeats increases, both the ultimate strength and strain increase (Figure 4c). Ultimate strength and strain of the 16xKLV-Mfp hydrogel reached 1.1 ± 0.3 MPa and 389 ± 78%, respectively. Furthermore, the tensile modulus of these hydrogels also increased with the number of silk-amyloid repeats. Overall, these tensile testing results revealed that a high β-sheet content is critical to the hydrogel's modulus, ultimate strength, and ultimate strain as it packs into β-crystals and forms

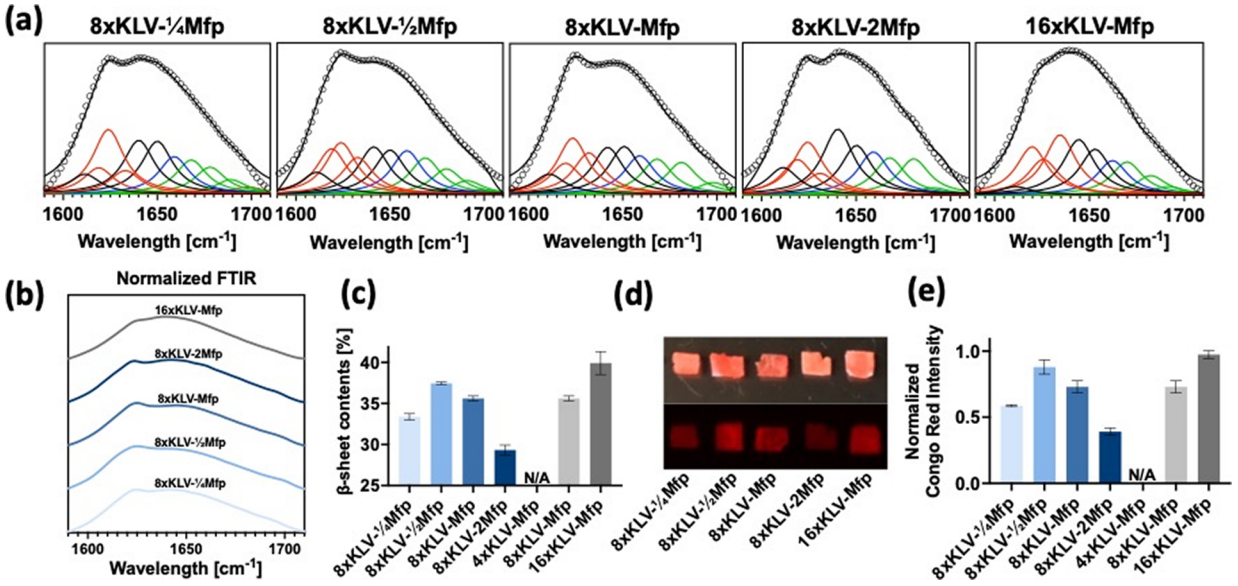

Figure 3. Structural characterization of SAM hydrogels. (a) FTIR spectra of SAM hydrogels and their deconvolutions. Black circles represent the FTIR data. Colored lines represent convolved components, with red and green lines representing the β-sheet and β-turn, respectively. Black lines at the top of each spectrum represent the sum of all deconvoluted functions. (b) Comparison of FTIR spectra between 1600 and 1700 cm^{-1} for all SAM hydrogels. (c) β-Sheet content of each SAM hydrogel estimated from FTIR spectra. (d) Images of Congo Red stained hydrogels. The top image is taken by a camera, and the bottom image is taken by fluorescence imager. (e) Normalized Congo Red intensity of each hydrogel.

https://doi.org/10.1021/acsami.3c12919
ACS Appl. Mater. Interfaces 2023, 15, 56786−56795

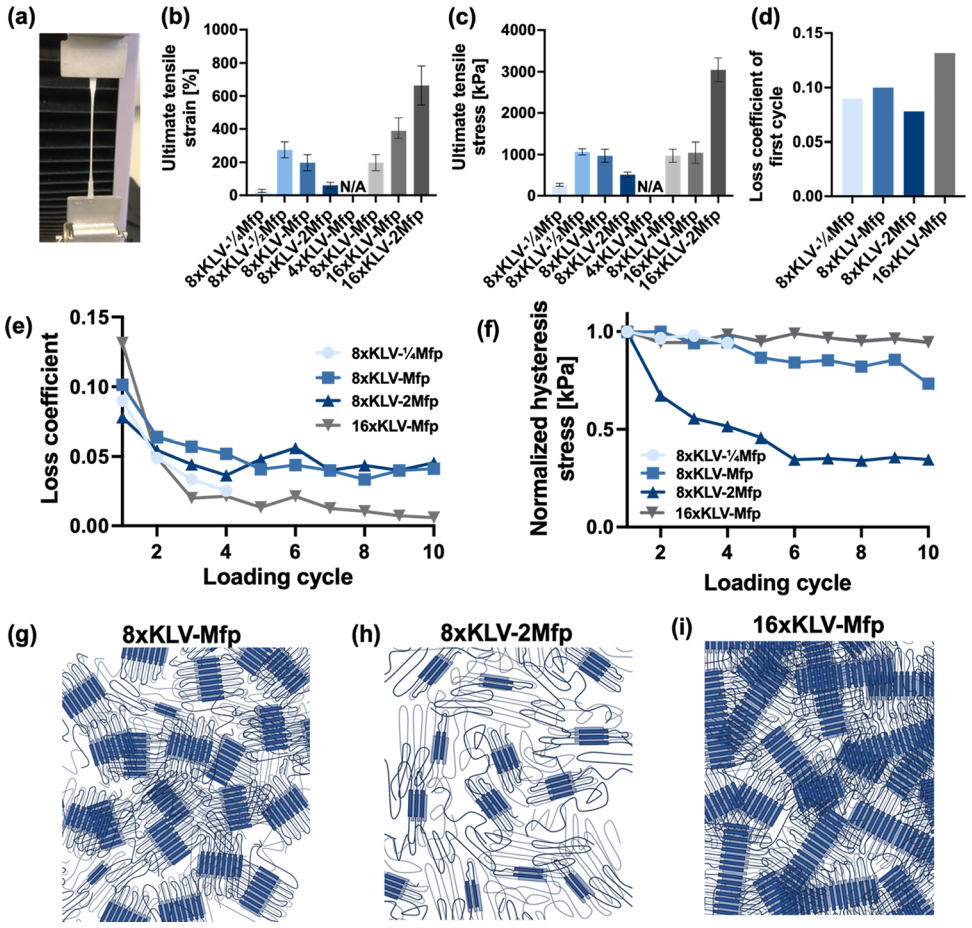

Figure 4. Mechanical properties of SAM hydrogels. (a) Photo showing a representative tensile testing experiment. (b) Breaking strain, (c) ultimate tensile stress, (d) hydrogel loss coefficient of the first pulling cycle, (e) hydrogel loss coefficient over 10 force loading/unloading cycles, (f) normalized hysteresis stress over 10 force loading/unloading cycles, and (g–i) schematic showing the hypothetical structures of (g) 8xKLV-Mfp, (h) 8xKLV-2Mfp and (i) 16xKLV-Mfp hydrogels.

strong intermolecular interactions within these β-crystals[21] (Figures 4g,i and S2). Furthermore, longer β-crystals increase spacing between the Mfp segments, hindering the intramolecular interaction of Mfp while promoting intermolecular interactions. This explains the superior mechanical property of the 16xKLV-2Mfp hydrogel in comparison to the 16xKLV-Mfp variant, demonstrated by its ultimate strength of 3 ± 0.3 MPa and an ultimate strain of 664 ± 119% (Figure 4b,c).

Next, we performed cyclic tensile tests to explore hydrogel hysteresis properties, which is vital for practical application[32,33] as it indicates how robustly these bioadhesives behave under repetitive force loading and unloading.[34,35] Based on the results, the 8xKLV-1/4Mfp hydrogel displayed deteriorating mechanical properties with force loading/unloading cycles and completely broke after the fourth cycle (Figures 4e,f and S3a). Similarly, the hysteresis stress of 8xKLV-2Mfp hydrogel decreased significantly with force loading/unloading cycles (Figures 4f and S3c). In contrast, hydrogels made of 8xKLV-Mfp and 16xKLV-Mfp showed a decrease in the hysteresis stress. The 16xKLV-Mfp hydrogel, in particular, displayed only a 5.4% decrease in hysteresis stress after 10 rounds of continuous force loading/unloading (Figures 4f and S3b,d). This robust cyclic mechanical performance is likely due to its high β-sheet content and crystallinity,[22,36] which enable reversible orientation during force loading/unloading. For hydrogels with a low β-sheet content, repeated loading/unloading cycles cause irreversible structural changes and material failure. Additionally, we calculated the loss coefficient of SAM hydrogels for each loading cycle (Figure S4c).[34] The SAM hydrogels exhibited a consistent lost coefficient of 0.1 ± 0.02 at the first loading cycle (Figure 4d), which aligns with that of collagen fibrils (Figure S4c).[34] These combination of properties make the 16xKLV-Mfp hydrogel a suitable candidate for biomedical applications such as cardiac materials needing high energy absorption and fatigue resistance.[37,38]

Adhesion, Stability, and Biocompatibility Tests of Different hydrogels. We examined the adhesion of the hydrogels to biological tissues. Porcine skin was used as the adherend substrate. Mfp domain located at the surface of SAM hydrogel can use a combination of molecular interactions to adhere to biological tissues, including cation–π interaction, π–π stacking, hydrogen bonding, and electrostatic interaction.[21] To mimic the wet biological conditions, all hydrogels were adhered between two skin samples when they were completely submerged underwater following published protocols (see Methods, Figure 5a). After adhesion, the "sandwich" structures were pulled in opposite directions until the skins were detached from one another. All SAM hydrogels failed adhesively (i.e., the hydrogel detached from one porcine skin sample while the hydrogels remained intact). This is consistent with the measured adhesive strengths being lower than the hydrogel ultimate tensile strengths for all SAM hydrogels. Hydrogels containing

https://doi.org/10.1021/acsami.3c12919
ACS Appl. Mater. Interfaces 2023, 15, 56786–56795

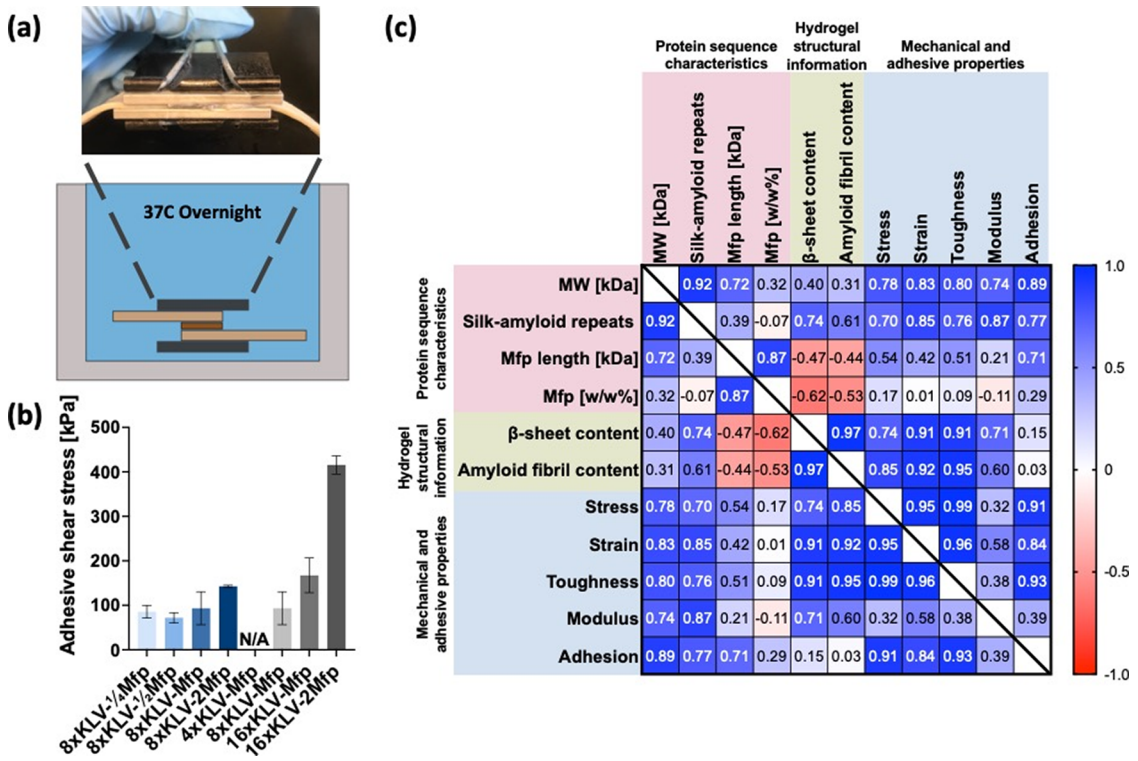

Figure 5. Underwater adhesively of SAM hydrogels. (a) Schematic showing a representative underwater adhesion setup. (b) Adhesion shear stress measured of different SAM hydrogels. (c) Correlation analysis between the protein sequence characteristics, hydrogel structure, and mechanical and adhesion properties.

8xKLV showed stronger adhesion strengths as Mfp length increases (Figure 5b), indicating that longer Mfp sequences enhance underwater adhesion. This is consistent with previous studies showing that Mfp is the major contributor to surface adhesion.[21] Surprisingly, for hydrogels containing full-length Mfp, their underwater adhesion increased when silk-amyloid repeats increased (Figure 5b). This is likely because proteins with a higher number of silk-amyloid repeats provide better separation between Mfp segments when folded into β-sheets, therefore displaying Mfp chains on hydrogel surfaces and enabling more effective interaction with surfaces (Figure 1b).[21]

Following the discovered trend, we expected the 16xKLV-2Mfp hydrogel to have a high adhesion strength. Indeed, the 16xKLV-2Mfp hydrogel displayed a high ultimate strength of 3 ± 0.3 MPa, an ultimate strain of 664 ± 119%, and an attractive adhesion of 416 ± 20 kPa to porcine skin even when fixed underwater. The measured adhesion of 16xKLV-2Mfp to biological tissue surface is significantly higher than previous works using nature-inspired tissue adhesives,[39−41] which would enable a wide range of biomedical applications.

Additionally, we performed a swelling test to evaluate the long-term stability of SAM hydrogel for biomedical applications. After incubating the SAM hydrogel in PBS buffer for 10 days, no detectable swelling was observed (<5%, Figure S5a). We further analyzed the hydrogel's structure after 10 days of incubation in a PBS buffer. FTIR showed little to no statistical difference between pre- and post-incubation (Figure S5b). Additionally, biocompatibility tests were performed using human endothelial cells (HUVECs). After incubating HUVECs with the 16KLV-Mfp hydrogel for 48 h, the cells displayed healthy morphology, similar to cells without incubation with the hydrogel (Figure S6). Cell proliferation tests were also performed, and the results indicated similar proliferation activities between cells with or without hydrogel incubation (Figure S6). Altogether, these results indicated that the SAM hydrogels are stable during incubation in aqueous solution (for at least 10 days) and biocompatible.

Sequence-Structure−Property Relationships of SAM Hydrogels. To obtain a quantitative understanding of SAM hydrogel sequence−structure−property relationships, we performed correlation analyses using all measured protein sequence characteristics (i.e., molecular weight, silk-amyloid repeats, Mfp length, and Mfp weight percentage, Supplementary Table S1), hydrogel structural information (i.e., β-sheet content from FTIR, amyloid fibril content from Congo Red staining, Supplementary Table S4), mechanical properties (i.e., ultimate tensile strength, ultimate strain, toughness, and modulus, Supplementary Table S5), and adhesive strength (Figure 5c). The correlation matrix shows that silk-amyloid repeats correlate strongly with amyloid fibril content (r = 0.61), which correlates positively with mechanical properties. Meanwhile, adhesive properties correlate strongly with protein MW (r = 0.89) and Mfp length (r = 0.71), but weakly with Mfp weight percentage (r = 0.29). The strong correlation between adhesion and protein MW is consistent with our previous observations, suggesting that high MW SAM proteins should be pursued in future designs to improve adhesion.[24] For hydrogels with fixed Mfp lengths, a high number of silk-amyloid repeats promote ultimate strength, ultimate strain, toughness, and adhesion. Additionally, given a fixed number of silk-amyloid repeats, increasing Mfp length beyond 1/2 Mfp promotes surface adhesion. Overall, we demonstrated that the mechanical and adhesive properties of SAM hydrogels can be tuned by engineering protein sequences, therefore enabling different applications.

https://doi.org/10.1021/acsami.3c12919
ACS Appl. Mater. Interfaces 2023, 15, 56786−56795

CONCLUSIONS AND DISCUSSION

Collectively, we have designed, biosynthesized, and characterized multiple novel SAM hydrogels in which proteins contain different combinations of β-sheet amyloid proteins, spidroins, and Mfp fragments. FITR and Congo red staining revealed hydrogel secondary structures and amyloid fibril content, respectively. Mechanical tests revealed their elongated and adhesion properties. These data allowed us to identify sequence-structure−property relationships for SAM hydrogels that can be used as design rules for bioadhesives. We found that (1) a long Mfp sequence on 8xKLV interferes with the β-sheet formation and weakens hydrogel mechanical properties. (2) Hydrogel surface adhesivity correlates more strongly with Mfp length than Mfp weight percent. (3) Hydrogel silk-amyloid repeats highly correlate with the hydrogel mechanical properties. As the number of silk-amyloid repeats increases, protein chains can fold into higher β-sheet amyloid content and more ordered β-crystals at a longer length scale, which allows stronger intermolecular interactions and thus leads to higher hydrogel strength and modulus.[21,36] Additionally, a more ordered amyloid structure allows Mfp segments to protrude outside the β-crystals and form intermolecular Mfp−Mfp interactions (Figure 4i). This results in higher ultimate strain and toughness under a tensile loading of the hydrogel (Figure 4f). On the other hand, proteins with low β-sheet content tend to form disordered oligomers or aggregates at short length scales, leading to hydrogels that break at low strain (Figure 4h). Considering the observed relationships, we anticipated that further increasing the number of silk-amyloid repeats may continue to promote ordered β-crystal assembly, which would increase hydrogel strength and ultimate strain while tolerating longer Mfp sequences (i.e., reducing the interference of Mfp on β-crystals folding) and increasing underwater adhesion. This trend may continue until a critical point where more silk-amyloid repeats cease to enhance β-sheet content (Figure 4g,h).

Among all SAM hydrogels tested in this work, the 16KLV-2Mfp hydrogel displayed the highest adhesivity (416 ± 20 kPa) and a high ultimate tensile strength (3.0 ± 0.3 MPa), surpassing many recombinant protein adhesives[42,43] and some chemical adhesives.[44−46] Most nature-derived and nature-inspired adhesive hydrogels have a low tensile strength. For instance, even with advanced cross-linking methods or double cross-linking, silk-derived hydrogels exhibited a tensile strength of 10−15 kPa,[47] and gelatin-based hydrogels had tensile strength less than 95 kPa.[48,49,50,51] In comparison, our 16KLV-2Mfp hydrogel displayed a tensile strength of 3.0 ± 0.3 MPa. Additionally, hydrogels made of naturally derived protein polymers such as chitosan, gelatin, and collagen showed adhesion of less than 100 kPa on wet tissue surfaces.[1,18,52,53] Similarly, the adhesion of some silk-based hydrogels and mussel-inspired polymers is also lower than 30 kPa.[4,54] In comparison, our 16KLV-2Mfp protein hydrogel exhibited an adhesion of 416 ± 20 kPa, substantially higher than those in previous reports.

While the SAM hydrogels can be potentially used in various biomedical settings, it is specifically suitable for repairing tendons-to-bone, as it possess the necessary adhesive and mechanical properties uniquely needed for this application.[21,46] Additionally, all tendon-to-bone repairs require casting or immobilization of the injured area for at least two weeks during postoperative rehabilitation.[55−57,58] SAM hydrogel can form adhesion on the treated area within 18 h of immobilization, shorter than the standard immobilization period.

At last, the design rules learned from this study can be potentially applied to engineering other protein-based adhesives for different applications. Our study also highlights the power of synthetic biology, which can be used not only to produce materials and chemicals[59−62] but also to study material sequence-property relationships and illuminate complicated molecular mechanisms.

METHODS

Chemicals and Reagents. Unless specifically mentioned, all chemicals and reagents were obtained from Millipore Sigma (St. Louis, MO, USA). Plasmid purification and gel extraction kits were purchased from iNtRON Biotechnology (Seoul, South Korea). FastDigest restriction enzymes and T4 DNA ligase were purchased from Thermo Fisher Scientific and were used according to manufacturer-suggested protocols. Ni-NTA columns and ion exchange columns for protein purification were purchased from GE Healthcare (Chicago, IL).

Strains and Growth Conditions. *E. coli* NEB10B strain was used in all plasmid cloning and protein expression experiments. For all cloning, *E. coli* cells were cultured in Luria broth medium (LB) containing 10 g/L tryptone, 5 g/L yeast extract, 10 g/L NaCl, and 100 μg/mL ampicillin with pH adjusted to 7.4.

Plasmid Construction. A SI-Brick system was used to facilitate the cloning of different SAM proteins. DNA sequences encoding 4xKLV were amplified from plasmids used in previous work[22] and incorporated into a standard expression vector with an arabinose-inducible pBAD promoter.[22] Recursive digestion and ligation using the NheI/BcuI restriction sites were performed to obtain pE8a-4xKLV, pE8a-8xKLV, pE8a-16xKLV variants.[21,22] The Mfp gene sequence amplified from plasmid pE7a-mfp51[24] and ligated into plasmids containing silk-amyloid, yielding pE8a-4xKLV-Mfp, pE8a-8xKLV-Mfp, pE8a-16xKLV-Mfp, pE8a-16xKLV-2Mfp.

Protein Expression. All proteins were expressed in *E. coli* NEB10β strain (New England Biolabs) following previously published methods.[63] Overnight cell cultures were used to inoculate newly prepared LB (10 g/L tryptone, 10 g/L sodium chloride, and 5 g/L yeast extract with 100 μg/ml ampicillin) media. Cells were induced with 0.4 w/v% arabinose at an OD_{600nm} of 2. Cells were harvested 8 h after induction by centrifugation at 3500g and stored at −80 °C until further use.

Protein Purification. Cell pellets were resuspended in lysis buffer (6 M guanidine chloride, 300 mM NaCl, 50 mM K_2HPO_4, pH = 7.4) and lysed by constant stirring for 6 h followed by centrifugation. The collected lysates were further sonicated on ice for 40 min with a QSonica probe sonicator using 5 s on/5 s off cycles. Cell lysates were filtered through 0.2 μm filter membranes, and the filtered supernatant was loaded to Ni-NTA columns (Millipore Sigma). After washing with 5−10 column volume (CV) of washing buffer (50 mM imidazole added to lysis buffer), proteins were eluted with 5−10 CV of elution buffer (250 imidazole added to lysis buffer). The eluted proteins were dialyzed against 1% acetic acid. The dialyzed proteins were lyophilized and stored at −80 °C until further use.

SDS-PAGE. Sodium dodecyl sulfate-polyacrylamide (SDS-PAGE) gels were cast in 1 mm-thick casting cases (Bio-Rad, Hercules, CA). The gels consist of a 14% polyacrylamide separating gel, which comprises 14% bisacrylamide, 375 mM tris pH = 8.8, 0.1% m/v sodium dodecyl sulfate (SDS), 0.1% m/v ammonium persulfate (APS), and 0.04% v/v tetramethylethlyenediamine (TEMED), and a 5% polyacrylamide stacking gel, which comprises 5% bisacrylamide, 125 mM tris pH = 6.8, 0.1% m/v SDS, 0.1% m/v APS, and 0.1% v/v TEMED. Purified proteins were loaded to each lane. The gels were run on Mini-PROTEAN Tetra Cells (Bio-Rad) in 1× TGS buffer (30 g/L tris, 144 g/L-glycine, and 10 g/L SDS) at 130−150 V for 80−120 min or until the blue dye front exits the gel. Gels were then stained in Coomassie Blue staining solution (40% v/v methanol, 7% v/v acetic acid, and 0.1% w/v Coomassie Brilliant Blue) for 30−60 min at room temperature with gentle agitation. Gels were destained in Coomassie Blue destaining solution (40% v/v methanol, 7% v/v acetic acid) for at

https://doi.org/10.1021/acsami.3c12919
ACS Appl. Mater. Interfaces 2023, 15, 56786−56795

least 60 min and imaged on an Azure c600 Imager (Azure Biosystems, Dublin, CA).

Hydrogel Preparation. Purified and lyophilized proteins were fully dissolved in 1,1,1,3,3,3-hexafluoroisopropanol (HFIP) to a protein concentration of 1−1.5% (w/v) in glass vials. Excess HFIP was evaporated to keep a final protein concentration of 7.5% w/v prior to the addition of a 2.5-fold volume of phosphate buffer (PBS, 100 mM sodium phosphates, 300 mM sodium chloride, pH 6). The solution was uniformly agitated, subsequently covered with parafilm, and incubated overnight for at least 12 h. The parafilm was then removed, and the solution was set under ambient conditions quiescently for another 8 h. Using forceps, the resulting hydrogel was peeled out of the mold and submerged in fresh phosphate buffer for at least 12 h to solvent-exchange any residual HFIP remaining within the hydrogel.

Mechanical Testing. Mechanical properties were measured by using an MTS Criterion Model 41 universal test frame fitted with a 25 N load cell (MTS Systems Corporation, Eden Prairie, MN). Hydrogel strength, strain, and toughness were measured by using a dogbone-shaped hydrogel. Tensile tests were performed after the hydrogels were removed from their storage phosphate buffer (100 mM sodium phosphates and 300 mM sodium chloride, pH 6). Tensile tests were conducted at a cross-head speed of 16 mm/min. The slope of initial elastic regions of a strain-stress curve was measured as Young's modulus. The ultimate tensile strength was calculated as the maximum load divided by the initial rectangular cross-sectional area of the middle section of the dog-bone. The ultimate strain was calculated as the percentage of hydrogel elongation relative to the initial length of the middle section of dog-bone in between tensometer grips (8 mm). The toughness was calculated by integrating the area under the strain-stress curve. For cyclic loading measurements, hydrogels made of different variants were prepared and mounted, as described above. To avoid dehydration of the hydrogels, all cyclic loading and unloading tests were performed in an environmental chamber with relative humidity control at 80−90%. Hydrogels were pulled at a rate of 16 mm/min beyond the yield point, returned to 0% elongation, and repeated over 10 cycles with no wait time in between. 8xKLV-1/4 Mfp, 8xKLV-Mfp, 8xKLV-2Mfp, and 16xKLV-Mfp hydrogels were strained up to 17, 60, 30, and 100%, respectively for cyclic test. For each protein variant, loss coefficients were calculated as the energy ratio between the loading and unloading curves over the total energy under the loading curve. The hysteresis of all cycles was calculated as the energy difference between the loading and unloading curves divided by the hydrogel volume.

Fourier Transform Infrared Spectroscopy. Hydrogels were flash-frozen in liquid nitrogen and lyophilized to preserve the secondary structures. FTIR spectra of the dried hydrogel samples were collected on a Thermo Nicolet Nexus 670 FTIR spectrometer (Thermo Fisher Scientific, Waltham, MA) fitted with a Golden Gate diamond ATR accessory. Spectra were acquired between 400 and 2000 cm^{-1}. A total of 128 scans were performed and obtained with the OMINIC software. Only the amide I band, between 1600 and 1700 cm^{-1}, was analyzed using the Fityk 0.9.8. software. A baseline was applied to each spectrum using a built-in convex hull algorithm. The baselined amide I band was deconvoluted into 11 distinct Lorentzian peaks centered at 1618.5, 1624.5, 1632.5, and 1700 cm^{-1} for the β-sheet, 1610, 1642, and 1651 cm^{-1} for random coil, 1659 cm^{-1} for α-helix, and 1666.5, 1678, and 1691 cm^{-1} for the β-turn. Peak centers were assigned based on those used in previous studies.[21,26,29,64] Peak areas were integrated, and area percentages were calculated as the individual peak areas over the sum of all peak areas.

Environmental Scanning Electron Microscopy (ESEM). Fresh protein hydrogels were frozen in liquid nitrogen and lyophilized. For sample measurement, freeze-dried hydrogels were mounted onto a stainless-steel sample holder by using black carbon tape. Samples were sputter-coated with 10 nm Au by using a Leica EM ACE600 high-vacuum sputter coater (Leica Microsystems, Wetzlar, Germany). The coated hydrogels (top-down morphologies and cross-sections) were imaged using an Environmental Scanning Electron Microscope, Quattro S ESEM (Thermofisher Scientific, Waltham, Massachusetts).

Underwater Adhesion Testing. Porcine skin samples were cut from a 20 cm × 20 cm sheet of porcine skin with a thickness of 1.524 ± 0.254 mm (I-188), purchased from Stellen Medical, LLC (St. Paul, MN, USA). Each piece of 1 cm × 5 cm porcine skin was used for adhesion tests and was completely immersed in 1× PBS for approximately 20−30 min to be thawed and equilibrated on its surface. The square-shaped, 10 mm × 10 mm SAM hydrogels were applied between two pieces of porcine skin samples while completely submerged in a water bath. A constant pressure of 100 kPa was applied by the binding clip to the adherend overlap area for 18 h at 37 °C. Adhesion properties were measured under ambient conditions by using an MTS Criterion Model 41 universal test frame fitted with a 25 N load cell (MTS Systems Corporation). Adhesion tests were conducted at a cross-head speed of 2 mm/min. The maximum force at fracture was divided by the area of the protein hydrogel to determine the adhesion strength.

Swelling Test. The 16xKLV-Mfp hydrogel was immersed in 1× PBS (pH 7.4) and maintained at 37 °C for a duration of 10 days. The size of the hydrogel was measured at regular 24 h intervals using a ruler. Following the swelling test, the hydrogel samples were collected and subjected to FTIR analysis using the abovementioned method.

Congo Red Analysis. Congo Red staining was performed following published methods.[30,31,65] All lyophilized SAM hydrogels were soaked in solution A (80% EtOH, saturated NaCl) for 10 min. The gels were removed and directly soaked in Solution B (80% EtOH, saturated NaCl, 1.1 mg/ml of saturated Congo Red stain) for 5 min. The gels were washed and dehydrated in 100% EtOH three times before being imaged on an Azure c600 Imager (Azure Biosystems, Dublin, CA). The intensity of Congo Red was quantified by using ImageJ.

Correlation Analysis. For linear relationship analyses, Pearson correlation coefficients r were calculated between each two variables using Prism 9.0 (GraphPad, San Diego, CA, United States) with a confidence interval of 95%. Colors were added for visualization, where blue denotes a r value of 1, and red indicates a r value of −1.

Cell Proliferation Assay. The study evaluated cell proliferation using BrdU colorimetric ELISA. HUVECs (1×10^4) were seeded per well in a 96-well culture format. The growth medium was added with or without the 16xKLV-Mfp SAM hydrogel. Detection of BrdU incorporation into newly synthesized DNA of actively proliferating cells was assessed using a multiwell spectrophotometer at 450 nm, following the manufacturer's instructions (abcam cat# ab126556). The assay was repeated in triplicate to ensure accuracy.

■ ASSOCIATED CONTENT

Data Availability Statement

All study data are included in the article and/or SI Appendix.

Supporting Information

The Supporting Information is available free of charge at https://pubs.acs.org/doi/10.1021/acsami.3c12919.

Sequence information, mechanical properties, adhesion properties, and hysteresis curves (PDF)

■ AUTHOR INFORMATION

Corresponding Author

Fuzhong Zhang − *Department of Energy, Environmental & Chemical Engineering, Institute of Materials Science and Engineering, and Division of Biological & Biomedical Sciences, Washington University in St. Louis, Saint Louis, Missouri 63130, United States;* orcid.org/0000-0001-6979-7909; Phone: +1 (314) 935-7671; Email: fzhang@seas.wustl.edu; Fax: +1 (314) 935-7211

Authors

Juya Jeon − *Department of Energy, Environmental & Chemical Engineering, Washington University in St. Louis, Saint Louis, Missouri 63130, United States;* orcid.org/0000-0001-7723-9413

Kok Zhi Lee − *Department of Energy, Environmental & Chemical Engineering, Washington University in St. Louis, Saint Louis, Missouri 63130, United States;* orcid.org/0000-0002-1836-2662
Xiaolu Zhang − *Department of Energy, Environmental & Chemical Engineering, Washington University in St. Louis, Saint Louis, Missouri 63130, United States*
John Jaeger − *Department of Energy, Environmental & Chemical Engineering, Washington University in St. Louis, Saint Louis, Missouri 63130, United States*
Eugene Kim − *Department of Energy, Environmental & Chemical Engineering, Washington University in St. Louis, Saint Louis, Missouri 63130, United States*
Jingyao Li − *Department of Energy, Environmental & Chemical Engineering, Washington University in St. Louis, Saint Louis, Missouri 63130, United States;* orcid.org/0000-0002-6834-4681
Larisa Belaygorod − *Department of Surgery, Section of Vascular Surgery, Washington University of Medicine in St. Louis, Saint Louis, Missouri 63110, United States*
Batool Arif − *Department of Surgery, Section of Vascular Surgery, Washington University of Medicine in St. Louis, Saint Louis, Missouri 63110, United States*
Guy M. Genin − *NSF Science and Technology Center for Engineering MechanoBiology, Department of Mechanical Engineering & Materials Science, Institute of Materials Science and Engineering, and Division of Biological & Biomedical Sciences, Washington University in St. Louis, Saint Louis, Missouri 63130, United States;* orcid.org/0000-0003-3612-4729
Marcus B. Foston − *Department of Energy, Environmental & Chemical Engineering, Washington University in St. Louis, Saint Louis, Missouri 63130, United States;* orcid.org/0000-0002-4227-0362
Mohamed A. Zayed − *Department of Surgery, Section of Vascular Surgery, Department of Radiology, Division of Molecular Cell Biology, and Division of Molecular Cell Biology, Washington University of Medicine in St. Louis, Saint Louis, Missouri 63110, United States; Veterans Affairs St. Louis Health Care System, St. Louis, Missouri 63106, United States*

Complete contact information is available at: https://pubs.acs.org/10.1021/acsami.3c12919

Notes

The authors declare no competing financial interest.

■ ACKNOWLEDGMENTS

This work was supported by the Office of Naval Research under the award number N0001419112126 awarded to F.Z. and the National Science Foundation under the award number DMR2105150 to M.F. and F.Z.

■ REFERENCES

(1) Zhu, W.; Chuah, Y. J.; Wang, D.-A. Bioadhesives for Internal Medical Applications: A Review. *Acta Biomaterialia* **2018**, *74*, 1−16.
(2) Zhu, H.; Tian, J.; Mao, H.; Gu, Z. Bioadhesives: Current Hotspots and Emerging Challenges. *Current Opinion in Biomedical Engineering* **2021**, *18*, No. 100271.
(3) Palacio, M. L. B.; Bhushan, B. Bioadhesion: A Review of Concepts and Applications. *Philos. Trans. R. Soc., A* **1967**, *2012* (370), 2321−2347.
(4) Pei, X.; Wang, J.; Cong, Y.; Fu, J. Recent Progress in Polymer Hydrogel Bioadhesives. *J. Polym. Sci.* **2021**, *59* (13), 1312−1337.
(5) Tzagiollari, A.; McCarthy, H. O.; Levingstone, T. J.; Dunne, N. J. Biodegradable and Biocompatible Adhesives for the Effective Stabilisation, Repair and Regeneration of Bone. *Bioengineering* **2022**, *9* (6), 250.
(6) Yuk, H.; Wu, J.; Sarrafian, T. L.; Mao, X.; Varela, C. E.; Roche, E. T.; Griffiths, L. G.; Nabzdyk, C. S.; Zhao, X. Rapid and Coagulation-Independent Haemostatic Sealing by a Paste Inspired by Barnacle Glue. *Nat Biomed Eng* **2021**, *5* (10), 1131−1142.
(7) Chen, X.; Zhang, J.; Chen, G.; Xue, Y.; Zhang, J.; Liang, X.; Lei, I. M.; Lin, J.; Xu, B. B.; Liu, J. Hydrogel Bioadhesives with Extreme Acid-Tolerance for Gastric Perforation Repairing. *Adv Funct Materials* **2022**, *32* (29), No. 2202285.
(8) Ma, C.; Sun, J.; Li, B.; Feng, Y.; Sun, Y.; Xiang, L.; Wu, B.; Xiao, L.; Liu, B.; Petrovskii, V. S.; Liu, B.; Zhang, J.; Wang, Z.; Li, H.; Zhang, L.; Li, J.; Wang, F.; Göstl, R.; Potemkin, I. I.; Chen, D.; Zeng, H.; Zhang, H.; Liu, K.; Herrmann, A. Ultra-Strong Bio-Glue from Genetically Engineered Polypeptides. *Nat. Commun.* **2021**, *12* (1), 3613.
(9) Liu, G.; Li, Y.; Yang, L.; Wei, Y.; Wang, X.; Wang, Z.; Tao, L. Cytotoxicity Study of Polyethylene Glycol Derivatives. *RSC Adv.* **2017**, *7* (30), 18252−18259.
(10) Pascual, G.; Sotomayor, S.; Rodríguez, M.; Pérez-Köhler, B.; Kühnhardt, A.; Fernández-Gutiérrez, M.; San Román, J.; Bellón, J. M. Cytotoxicity of Cyanoacrylate-Based Tissue Adhesives and Short-Term Preclinical In Vivo Biocompatibility in Abdominal Hernia Repair. *PLoS ONE* **2016**, *11* (6), No. e0157920.
(11) Zhang, H.; Zhao, T.; Duffy, P.; Dong, Y.; Annaidh, A. N.; O'Cearbhaill, E.; Wang, W. Hydrolytically Degradable Hyperbranched PEG-Polyester Adhesive with Low Swelling and Robust Mechanical Properties. *Adv. Healthcare Mater.* **2015**, *4* (15), 2260−2268.
(12) Bhagat, V.; Becker, M. L. Degradable Adhesives for Surgery and Tissue Engineering. *Biomacromolecules* **2017**, *18* (10), 3009−3039.
(13) Azadani, A. N.; Matthews, P. B.; Ge, L.; Shen, Y.; Jhun, C.-S.; Guy, T. S.; Tseng, E. E. Mechanical Properties of Surgical Glues Used in Aortic Root Replacement. *The Annals of Thoracic Surgery* **2009**, *87* (4), 1154−1160.
(14) Rathi, S.; Saka, R.; Domb, A. J.; Khan, W. Protein-Based Bioadhesives and Bioglues. *Polym Adv Technol* **2019**, *30* (2), 217−234.
(15) Katyal, P.; Mahmoudinobar, F.; Montclare, J. K. Recent Trends in Peptide and Protein-Based Hydrogels. *Current Opinion in Structural Biology* **2020**, *63*, 97−105.
(16) Sun, J.; Han, J.; Wang, F.; Liu, K.; Zhang, H. Bioengineered Protein-based Adhesives for Biomedical Applications. *Chem.-Eur. J.* **2022**, *28* (1), No. e202102902.
(17) Sun, J.; Su, J.; Ma, C.; Göstl, R.; Herrmann, A.; Liu, K.; Zhang, H. Fabrication and Mechanical Properties of Engineered Protein-Based Adhesives and Fibers. *Adv. Mater.* **2020**, *32* (6), No. 1906360.
(18) Lee, K. Z.; Jeon, J.; Jiang, B.; Subramani, S. V.; Li, J.; Zhang, F. Protein-Based Hydrogels and Their Biomedical Applications. *Molecules* **2023**, *28* (13), 4988.
(19) Li, F.; Ye, L.; Zhang, L.; Li, X.; Liu, X.; Zhu, J.; Li, H.; Pang, H.; Yan, Y.; Xu, L.; Yang, M.; Yan, J. Design of a Genetically Programmed Barnacle-Curli Inspired Living-Cell Bioadhesive. *Materials Today Bio* **2022**, *14*, No. 100256.
(20) Jeon, J.; Subramani, S. V.; Lee, K. Z.; Jiang, B.; Zhang, F. Microbial Synthesis of High-Molecular-Weight, Highly Repetitive Protein Polymers. *IJMS* **2023**, *24* (7), 6416.
(21) Kim, E.; Jeon, J.; Zhu, Y.; Hoppe, E. D.; Jun, Y.-S.; Genin, G. M.; Zhang, F. A Biosynthetic Hybrid Spidroin-Amyloid-Mussel Foot Protein for Underwater Adhesion on Diverse Surfaces. *ACS Appl. Mater. Interfaces* **2021**, *13* (41), 48457−48468.
(22) Dai, B.; Sargent, C. J.; Gui, X.; Liu, C.; Zhang, F. Fibril Self-Assembly of Amyloid−Spider Silk Block Polypeptides. *Biomacromolecules* **2019**, *20* (5), 2015−2023.
(23) Li, J.; Zhang, F. Amyloids as Building Blocks for Macroscopic Functional Materials: Designs, Applications and Challenges. *IJMS* **2021**, *22* (19), 10698.
(24) Kim, E.; Dai, B.; Qiao, J. B.; Li, W.; Fortner, J. D.; Zhang, F. Microbially Synthesized Repeats of Mussel Foot Protein Display

Enhanced Underwater Adhesion. *ACS Appl. Mater. Interfaces* **2018**, *10* (49), 43003−43012.
(25) Kim, E.; Qin, X.; Qiao, J. B.; Zeng, Q.; Fortner, J. D.; Zhang, F. Graphene Oxide/Mussel Foot Protein Composites for High-Strength and Ultra-Tough Thin Films. *Sci Rep* **2020**, *10* (1), 19082.
(26) Bowen, C. H.; Dai, B.; Sargent, C. J.; Bai, W.; Ladiwala, P.; Feng, H.; Huang, W.; Kaplan, D. L.; Galazka, J. M.; Zhang, F. Recombinant Spidroins Fully Replicate Primary Mechanical Properties of Natural Spider Silk. *Biomacromolecules* **2018**, *19* (9), 3853−3860.
(27) Li, J.; Jiang, B.; Chang, X.; Yu, H.; Han, Y.; Zhang, F. Bi-Terminal Fusion of Intrinsically-Disordered Mussel Foot Protein Fragments Boosts Mechanical Strength for Protein Fibers. *Nat Commun* **2023**, *14* (1), 2127.
(28) Lee, T. S.; Krupa, R. A.; Zhang, F.; Hajimorad, M.; Holtz, W. J.; Prasad, N.; Lee, S. K.; Keasling, J. D. BglBrick Vectors and Datasheets: A Synthetic Biology Platform for Gene Expression. *J Biol Eng* **2011**, *5* (1), 12.
(29) Lawrence, B. D.; Omenetto, F.; Chui, K.; Kaplan, D. L. Processing Methods to Control Silk Fibroin Film Biomaterial Features. *J. Mater. Sci.* **2008**, *43* (21), 6967−6985.
(30) Puchtler, H.; Sweat, F.; Levine, M. ON THE BINDING OF CONGO RED BY AMYLOID. *J Histochem Cytochem.* **1962**, *10* (3), 355−364.
(31) Yakupova, E. I.; Bobyleva, L. G.; Vikhlyantsev, I. M.; Bobylev, A. G. Congo Red and Amyloids: History and Relationship. *Bioscience Reports* **2019**, *39* (1), No. BSR20181415.
(32) Zhu, Y.; Zhang, Q.; Shi, X.; Han, D. Hierarchical Hydrogel Composite Interfaces with Robust Mechanical Properties for Biomedical Applications. *Adv. Mater.* **2019**, *31* (45), No. 1804950.
(33) Fuchs, S.; Shariati, K.; Ma, M. Specialty Tough Hydrogels and Their Biomedical Applications. *Adv. Healthcare Mater.* **2020**, *9* (2), No. 1901396.
(34) Liu, J.; Das, D.; Yang, F.; Schwartz, A. G.; Genin, G. M.; Thomopoulos, S.; Chasiotis, I. Energy Dissipation in Mammalian Collagen Fibrils: Cyclic Strain-Induced Damping, Toughening, and Strengthening. *Acta Biomaterialia* **2018**, *80*, 217−227.
(35) Zhang, X.; Lou, Z.; Yang, X.; Chen, Q.; Chen, K.; Feng, C.; Qi, J.; Luo, Y.; Zhang, D. Fabrication and Characterization of a Multilayer Hydrogel as a Candidate for Artificial Cartilage. *ACS Appl. Polym. Mater.* **2021**, *3* (10), 5039−5050.
(36) Li, J.; Zhu, Y.; Yu, H.; Dai, B.; Jun, Y.-S.; Zhang, F. Microbially Synthesized Polymeric Amyloid Fiber Promotes β-Nanocrystal Formation and Displays Gigapascal Tensile Strength. *ACS Nano* **2021**, *15* (7), 11843−11853.
(37) Li, M.; Pan, G.; Zhang, H.; Guo, B. Hydrogel Adhesives for Generalized Wound Treatment: Design and Applications. *J. Polym. Sci.* **2022**, *60* (8), 1328−1359.
(38) He, Y.; Li, Q.; Chen, P.; Duan, Q.; Zhan, J.; Cai, X.; Wang, L.; Hou, H.; Qiu, X. A Smart Adhesive Janus Hydrogel for Non-Invasive Cardiac Repair and Tissue Adhesion Prevention. *Nat Commun* **2022**, *13* (1), 7666.
(39) Zhang, L.; Liu, M.; Zhang, Y.; Pei, R. Recent Progress of Highly Adhesive Hydrogels as Wound Dressings. *Biomacromolecules* **2020**, *21* (10), 3966−3983.
(40) Chen, Y.; Qin, H.; Mensaha, A.; Wang, Q.; Huang, F.; Wei, Q. Biomimetic Nanocomposite Hydrogel Networks for Robust Wet Adhesion to Tissues. *Composites Part B: Engineering* **2021**, *222*, No. 109071.
(41) Yuen, H. Y.; Bei, H. P.; Zhao, X. Underwater and Wet Adhesion Strategies for Hydrogels in Biomedical Applications. *Chemical Engineering Journal* **2022**, *431*, No. 133372.
(42) Ninan, L. Adhesive Strength of Marine Mussel Extracts on Porcine Skin. *Biomaterials* **2003**, *24* (22), 4091−4099.
(43) Brennan, M. J.; Kilbride, B. F.; Wilker, J. J.; Liu, J. C. A Bioinspired Elastin-Based Protein for a Cytocompatible Underwater Adhesive. *Biomaterials* **2017**, *124*, 116−125.
(44) Chen, L. X.; Coulombe, M.; Barthelat, F.; Rammal, A.; Mongeau, L.; Kost, K. Investigation of Surgical Adhesives for Vocal Fold Wound Closure. *The Laryngoscope* **2019**, *129* (9), 2139−2146.
(45) Avgoulas, E. I.; Sutcliffe, M. P. F.; Linderman, S. W.; Birman, V.; Thomopoulos, S.; Genin, G. M. Adhesive-Based Tendon-to-Bone Repair: Failure Modelling and Materials Selection. *J. R. Soc. Interface.* **2019**, *16* (153), No. 20180838.
(46) Linderman, S. W.; Golman, M.; Gardner, T. R.; Birman, V.; Levine, W. N.; Genin, G. M.; Thomopoulos, S. Enhanced Tendon-to-Bone Repair through Adhesive Films. *Acta Biomaterialia* **2018**, *70*, 165−176.
(47) Kim, S. H.; Yeon, Y. K.; Lee, J. M.; Chao, J. R.; Lee, Y. J.; Seo, Y. B.; Sultan, Md. T.; Lee, O. J.; Lee, J. S.; Yoon, S.; Hong, I.-S.; Khang, G.; Lee, S. J.; Yoo, J. J.; Park, C. H. Precisely Printable and Biocompatible Silk Fibroin Bioink for Digital Light Processing 3D Printing. *Nat Commun* **2018**, *9* (1), 1620.
(48) Zhao, P.; Wei, K.; Feng, Q.; Chen, H.; Wong, D. S. H.; Chen, X.; Wu, C.-C.; Bian, L. Mussel-Mimetic Hydrogels with Defined Cross-Linkers Achieved via Controlled Catechol Dimerization Exhibiting Tough Adhesion for Wet Biological Tissues. *Chem. Commun.* **2017**, *53* (88), 12000−12003.
(49) Lee, Y.; Bae, J. W.; Oh, D. H.; Park, K. M.; Chun, Y. W.; Sung, H.-J.; Park, K. D. In Situ Forming Gelatin-Based Tissue Adhesives and Their Phenolic Content-Driven Properties. *J. Mater. Chem. B* **2013**, *1* (18), 2407.
(50) Jacob, R. S.; Ghosh, D.; Singh, P. K.; Basu, S. K.; Jha, N. N.; Das, S.; Sukul, P. K.; Patil, S.; Sathaye, S.; Kumar, A.; Chowdhury, A.; Malik, S.; Sen, S.; Maji, S. K. Self Healing Hydrogels Composed of Amyloid Nano Fibrils for Cell Culture and Stem Cell Differentiation. *Biomaterials* **2015**, *54*, 97−105.
(51) Hu, B.; Shen, Y.; Adamcik, J.; Fischer, P.; Schneider, M.; Loessner, M. J.; Mezzenga, R. Polyphenol-Binding Amyloid Fibrils Self-Assemble into Reversible Hydrogels with Antibacterial Activity. *ACS Nano* **2018**, *12* (4), 3385−3396.
(52) Yang, L.; Li, H.; Yao, L.; Yu, Y.; Ma, G. Amyloid-Based Injectable Hydrogel Derived from Hydrolyzed Hen Egg White Lysozyme. *ACS Omega* **2019**, *4* (5), 8071−8080.
(53) Khanlari, S.; Dubé, M. A. Bioadhesives: A Review: Bioadhesives: A Review. *Macromol. React. Eng.* **2013**, *7* (11), 573−587.
(54) Pei, X.; Zhang, H.; Zhou, Y.; Zhou, L.; Fu, J. Stretchable, Self-Healing and Tissue-Adhesive Zwitterionic Hydrogels as Strain Sensors for Wireless Monitoring of Organ Motions. *Mater. Horiz.* **2020**, *7* (7), 1872−1882.
(55) Bunker, D. L. J.; Ilie, V.; Ilie, V.; Nicklin, S. Tendon to Bone Healing and Its Implications for Surgery. *Muscles Ligaments Tendons J.* **2014**, *4* (3), 343−350.
(56) Braunstein, M.; Baumbach, S. F.; Boecker, W.; Carmont, M. R.; Polzer, H. Development of an Accelerated Functional Rehabilitation Protocol Following Minimal Invasive Achilles Tendon Repair. *Knee Surg Sports Traumatol Arthrosc* **2018**, *26* (3), 846−853.
(57) Thomopoulos, S.; Parks, W. C.; Rifkin, D. B.; Derwin, K. A. Mechanisms of Tendon Injury and Repair. *Journal Orthopaedic Research* **2015**, *33* (6), 832−839.
(58) Pneumaticos, S. G.; Noble, P. C.; McGarvey, W. C.; Mody, D. R.; Trevino, S. G. The Effects of Early Mobilization in the Healing of Achilles Tendon Repair. *Foot Ankle Int.* **2000**, *21* (7), 551−557.
(59) Jiang, W.; Qiao, J. B.; Bentley, G. J.; Liu, D.; Zhang, F. Modular Pathway Engineering for the Microbial Production of Branched-Chain Fatty Alcohols. *Biotechnol Biofuels* **2017**, *10* (1), 244.
(60) Bowen, C. H.; Sargent, C. J.; Wang, A.; Zhu, Y.; Chang, X.; Li, J.; Mu, X.; Galazka, J. M.; Jun, Y.-S.; Keten, S.; Zhang, F. Microbial Production of Megadalton Titin Yields Fibers with Advantageous Mechanical Properties. *Nat Commun* **2021**, *12* (1), 5182.
(61) Nguyen, P. Q.; Courchesne, N.-M. D.; Duraj-Thatte, A.; Praveschotinunt, P.; Joshi, N. S. Engineered Living Materials: Prospects and Challenges for Using Biological Systems to Direct the Assembly of Smart Materials. *Adv. Mater.* **2018**, *30* (19), No. 1704847.
(62) Jiang, W.; Gu, P.; Zhang, F. Steps towards 'Drop-in' Biofuels: Focusing on Metabolic Pathways. *Current Opinion in Biotechnology* **2018**, *53*, 26−32.

https://doi.org/10.1021/acsami.3c12919
ACS Appl. Mater. Interfaces 2023, 15, 56786−56795

(63) Bai, W.; Sargent, C. J.; Choi, J.-M.; Pappu, R. V.; Zhang, F. Covalently-Assembled Single-Chain Protein Nanostructures with Ultra-High Stability. *Nat Commun* **2019**, *10* (1), 3317.
(64) Wang, Q.; McArdle, P.; Wang, S. L.; Wilmington, R. L.; Xing, Z.; Greenwood, A.; Cotten, M. L.; Qazilbash, M. M.; Schniepp, H. C. Protein Secondary Structure in Spider Silk Nanofibrils. *Nat Commun* **2022**, *13* (1), 4329.
(65) Westermark, G. T.; Johnson, K. H.; Westermark, P. [1] Staining Methods for Identification of Amyloid in Tissue. In *Methods in Enzymology*; Elsevier, 1999; Vol. *309*, pp 3−25.

https://doi.org/10.1021/acsami.3c12919
ACS Appl. Mater. Interfaces 2023, 15, 56786−56795